JOURNAL OF MATERIALS SCIENCE 29 (1994) 2939–2943

Thermophysical studies on the substitution of Al^{3+} in gallium iron garnets

M. R. SALEM, E. ELSHEREAFY
Faculty of Science, El-Menoufia University, Egypt
M. M. ABOU SEKKINA*
Faculty of Science, Tanta University, Tanta, Egypt

Gallium iron garnet and its Al^{3+}-substituted derivatives have been prepared and sintered under oxygen pressure. On these materials, measurements were taken of infrared spectra, X-ray diffraction analysis, differential thermal analysis and the temperature dependence of d.c. electrical conductivity. The results obtained are explained, interpreted, compared and discussed in detail on the basis of structural conformation and the conduction mechanism prevailing.

1. Introduction

The interest of the present investigation lies in the useful application of ferromagnetic garnets in the production of memory cores, ferromagnets and microwave devices [1]. Since the discovery of ferrimagnetic garnets [2, 3], the interest in these materials has spread rapidly, although little work has been done on them. In recent years there has been great interest in the ferrospinels and perovskites which are very different from garnets. The latter are structurally more stable and the garnet structure appears to be quite selective and not efficiently packed [4].

The purpose of the present work was to investigate the thermal stability and electrical properties of Al^{3+}-substituted gallium–iron garnets to throw light on their physico-chemical properties.

2. Experimental procedure

2.1. Materials

The starting materials used in the present study were Ga_2O_3, Al_2O_3 and Fe_2O_3 of pure chemical grade (purity > 99.9%).

2.2. Material synthesis and sample preparation

Normal $Ga_3Fe_5O_{12}$ and stepwise Al^{3+}-substituted gallium–iron garnets in place of Ga^{3+} to aluminium–iron garnet ($Al_3Fe_5O_{12}$) were synthesized using the ceramic technique. This involves thoroughly grinding and pressing proportional amounts of component oxides, then firing at 1000 °C for 3 h followed by sintering at 1400 °C for 5 h under a stream of compressed oxygen atmosphere with intermediate grinding.

2.3. X-ray diffraction analysis

X-ray diffraction (XRD) analysis was undertaken using a Shimadzu (Japan) X-ray diffractometer type XD-3, with CuK_α radiation and a nickel filter, at room temperature in the range $2\theta = 10°$–$50°$.

2.4. Infrared absorption spectra measurements

The infrared absorption spectra were recorded using the solid KBr technique in the range 4000–200 cm^{-1}. A 598-Perkin–Elmar IR spectrophotometer was employed at room temperature.

2.5. Differential thermal analysis

Differential thermal analysis (DTA) was carried out using a Shimadzu DT-30 thermal analyser (Shimadzu, Kyoto, Japan) from room temperature up to 1000 °C under ambient atmosphere.

2.6. D.c. electrical conductivity measurements versus temperature

The d.c. electrical conductivity of garnet specimens was measured using the two-probe method. A Kiethley 175 autoranging electrometer, type Super Megohmeter Model RM-170 of very high input impedance ($10^{17}\Omega$cm) and graphite paste contacts were employed. Measurements were conducted in air at room and elevated temperatures up to $\simeq$ 500 K. The readings were often taken three times after 15 min for each temperature equilibration. The d.c. conductivity of the test samples was calculated from the relation

$$\sigma = \frac{d}{A}\frac{I}{V} \quad (1)$$

where d and A are the length (cm) and cross-sectional area (cm^2) of the test specimen, I(A) is the current passed, and V(V) is the constant d.c. voltage, applied.

*Author to whom all correspondence should be addressed.

0022–2461

3. Results and discussion

A fundamental study of refractory garnets reveals the infrared spectrum in the region between 1100 and 200 cm^{-1} which was more informative for these oxide compositions than the conventional rock salt regions.

The characteristic infrared absorption bands for all of Al^{3+}-substituted garnets suffer no shift of the main intense bands with Al^{3+} substitution in place of Ga^{3+} sites (see Fig. 1). This could plausibly be due to the great similarity of cationic radii for both Al^{3+} and Ca^{3+} because of d-block contraction in between the two elements in the Periodic Table. This, together with no change in the crystalline structure amongst the investigated garnets, causes no infrared band shift.

On the other hand, the strong infrared absorption bands suffer progressive weakening and broadening with Al^{3+} doping until complete disappearance in some cases (see Fig. 1 and Table I). This could be attributed to progressive mass changes and the propagated decrease in the degree of crystallinity caused by lattice imperfection which may lead to a defective crystal lattice. This attribution was further supported by results of X-ray diffraction analysis (see Fig. 2).

Thus the strong intensity vibration band observed for each of the garnet samples is most probably due to metal–oxygen vibrations. This is highly characteristic for garnet structures [5–7] depending on the variant valency cationic localities in the garnet crystalline lattice sites.

Fig. 2 shows the room-temperature CuK_α X-ray diffraction patterns of $Ga_3Fe_5O_{12}$ and its Al^{3+}-implanted gallium–iron garnets. The corresponding values of Bragg angles (2θ), interplanar spacings together with relative intensities ($I/I_0 \times 100$) are listed in Table II. It can easily be seen from Fig. 2 and Table II that there is a progressive slight decrease in the interplanar spacings as a function of Al^{3+} substitution in place of Ga^{3+}, and hence lattice contraction of the unit cell may occur. Because there is no marked difference in ionic radii of Ga^{3+} and Al^{3+}, this could plausibly be due to the increased lattice compactness in the same direction of Al^{3+} substitution.

On the other hand, the characteristic X-ray diffraction peaks progressively suffer weakening and broadening as a function of Al^{3+} substitution in place of Ga^{3+} in the different investigated garnets (see Fig. 2). This could plausibly be ascribed to the progressively decreased degree of crystallinity caused by doping-induced lattice imperfection in the garnet lattice. Of course the latter (lattice imperfection) may result in a defective and strained crystal lattice. It is of importance to deduce that because pattern 3 of Fig. 2 reflects the sharpest and highest intensity X-ray peaks

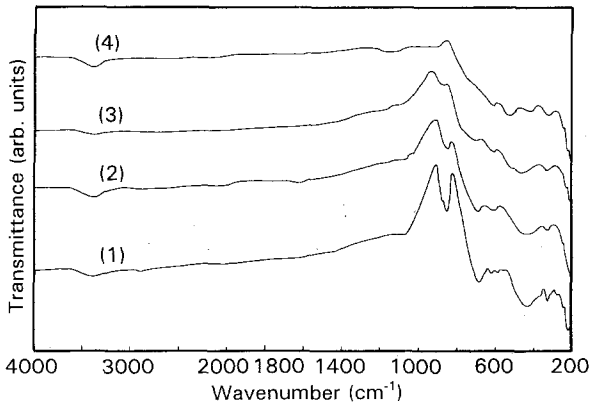

Figure 1 The room-temperature infrared absorption spectra of (1) $Ga_3Fe_5O_{12}$, (2) $Ga_2AlFe_5O_{12}$, (3) $GaAl_2Fe_5O_{12}$ and (4) $Al_3Fe_5O_{12}$ garnets.

TABLE I Band centres of characteristic absorption bands

Compound	Crystal structure	Absorption band wave number (cm^{-1})
$Ga_3Fe_5O_{12}$	Cubic	1080 w 870 s 690 m 637 v.w 445 sb 330 sp
$Ga_2AlFe_5O_{12}$	Distorted cubic	1070 v.w 870 m 690 m 637 w.b 650 b
$GaAl_2Fe_5O_{12}$	Pseudocubic	865 sh 720 w 620 w 650 b 335 w
$Al_3Fe_5O_{12}$	Cubic	620 wsh 520 m.b 420 w 330 w

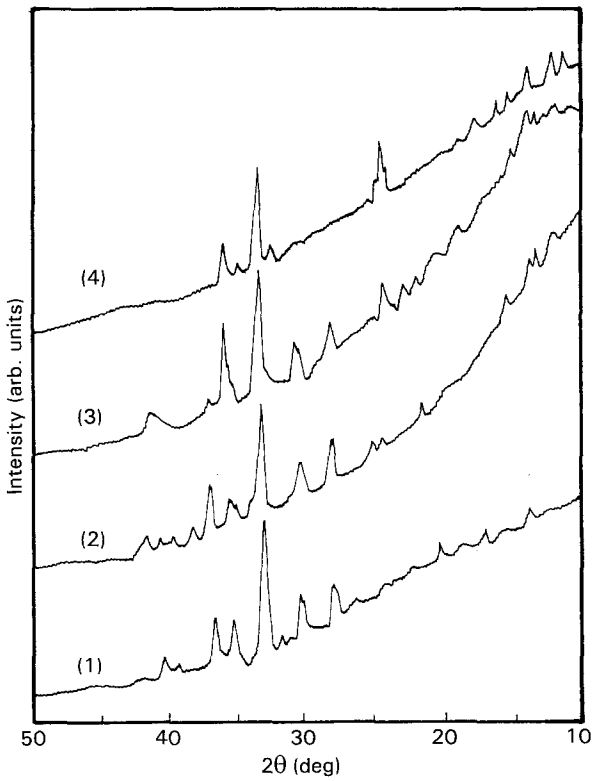

Figure 2 The room-temperature X-ray diffraction patterns of (1) $Ga_3Fe_5O_{12}$, (2) $Ga_2AlFe_5O_{12}$, (3) $GaAl_2Fe_5O_{12}$ and (4) $Al_3Fe_5O_{12}$ garnets.

TABLE II The evaluated X-ray diffraction analysis data for the various prepared and substituted garnets with those of the ASTM card of $Y_3Fe_5O_{12}$ garnet (for matching)

ASTM card			$Ga_3Fe_5O_{12}$			$Ga_2AlFe_5O_{12}$			$Ga_3Al_2Fe_5O_{12}$			$Al_3Fe_5O_{12}$		
d(nm)	$\frac{I}{I_0}$	hkl	d(nm)	$\frac{I}{I_0}$	hkl	d(nm)	$\frac{I}{I_0}$	hkl	d(nm)	$\frac{I}{I_0}$	hkl	d(nm)	$\frac{I}{I_0}$	hkl
0.52401	35	211	0.31828	34	400	0.31828	48	400	0.31498	40	400	0.36290	66	321
0.41139	10	220	–	–	–	–	–	–	–	–	–	–	–	–
0.33563	20	321	0.29751	36	421	0.29274	40	421	0.29274	33	421	0.26718	100	320
0.31314	30	400	–	–	–	–	–	–	–	–	–	–	–	–
0.25707	25	422	0.27111	100	320	0.26718	100	320	0.26718	100	320	0.25606	26	422
0.24553	6	431	–	–	–	–	–	–	–	–	–	–	–	–
0.23027	30	521	0.25606	37	422	0.25257	31	422	0.24918	73	422	0.24918	48	431
0.22147	6	440	0.24267	46	431	–	–	–	–	–	–	–	–	–
0.20283	30	611	0.22247	30	440	0.24267	48	431	–	–	–	–	–	–
0.18532	2	631	–	–	–	–	–	–	–	–	–	–	–	–

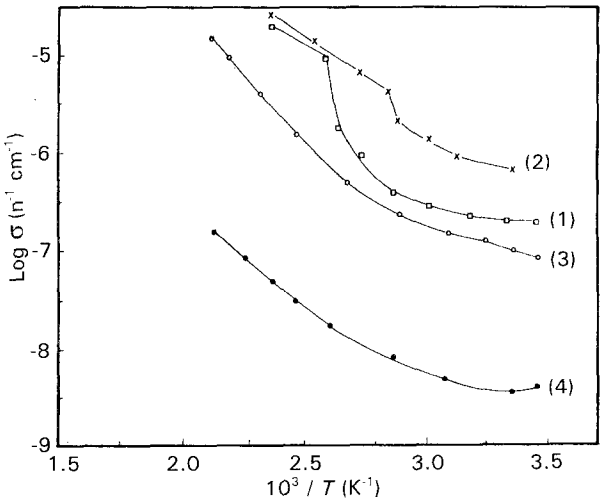

Figure 3 The variation of electrical conductivity, log σ, with temperature, $1000/T\,K^{-1}$, for (1) $Ga_3Fe_5O_{12}$, (2) $Ga_2AlFe_5O_{12}$, (3) $GaAl_2Fe_5O_{12}$ and (4) $Al_3Fe_5O_{12}$ garnets.

TABLE III Thermodynamic and kinetic data for various garnets

Garnet	E(kJ mol^{-1})	Order of reaction, n
$Ga_3Fe_5O_{12}$	1.86	1.022
$Ga_2AlFe_5O_{12}$	1.72	1.014
$GaAl_2Fe_5O_{12}$	1.59	1.134
$Al_3Fe_5O_{12}$	1.84	1.022

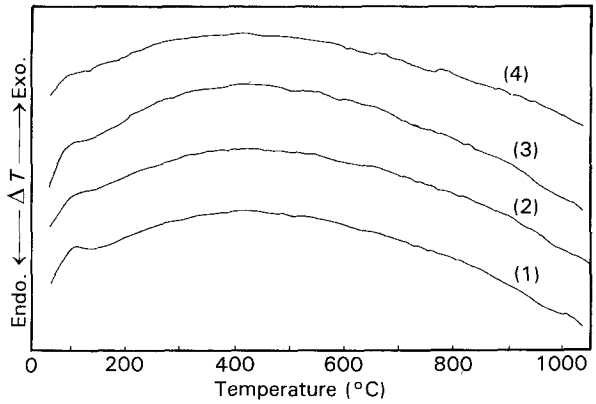

Figure 4 Differential thermal analysis of (1) $Ga_3Fe_5O_{12}$, (2) $Ga_2AlFe_5O_{12}$, (3) $GaAl_2Fe_5O_{12}$ and (4) $Al_3Fe_5O_{12}$ garnets.

of all other patterns investigated, it thus has the highest degree of crystallinity. Alternatively, Ga–$Al_2Fe_5O_{12}$ constitutes the optimum garnet composition.

Fig. 3 shows the variation of logarithmic electrical conductivity, log σ, versus reciprocal of absolute temperature, $1000/T\,K^{-1}$, for the prepared and sintered garnets. Plots for an Arrhenius equation type were applied, for which

$$\sigma = \sigma_0 e^{-E_g/2kT} \quad (2)$$

where σ is the electrical conductivity at temperature T, σ_0 is the pre-exponential constant, E_g is the energy gap (eV), k is the Boltzmann's constant, and T is the absolute temperature of each reading. The energy gap (activation energy, E_g) for conduction is evaluated and compiled in Table III.

Because all relations in Fig. 4 display a positive $d\sigma/dT$, our garnets are semi-conductors in the investigated temperature range. The present garnets are prepared and sintered under a stream of oxygen pressure, thus further oxygen diffusion may induce higher iron valencies (Fe^{3+}, Fe^{4+}, ..., etc.). This may enhance electronic transitions amongst the iron cations whether in tetrahedral, octahedral or dodecahedral lattice sites. Comparing the present data with previous author's data [8] indicates that our investigated samples display relatively higher conductivity and lower activation energy values for conduction. Consequently, the present prepared and sintered garnets are highly modified. It was noticed as a general trend that the electrical conductivity values become lower and values of energy gap (E_g, eV) become progressively higher with Al^{3+} substitution in place of Ga^{3+}. Accordingly, it was concluded that the electronic band model is the predominant mechanism for electrical conduction in the garnet bodies.

The electrical conductivity in the relatively low temperature range of each plot (Fig. 3) is due to an extrinsic conduction mechanism and the conduction in the higher temperature range is due to an intrinsic conduction mechanism; consequently, the inflection of the conductivity curves (Fig. 3) between the lower and higher temperature ranges could be highly correlated with change in the mode of electrical conduction.

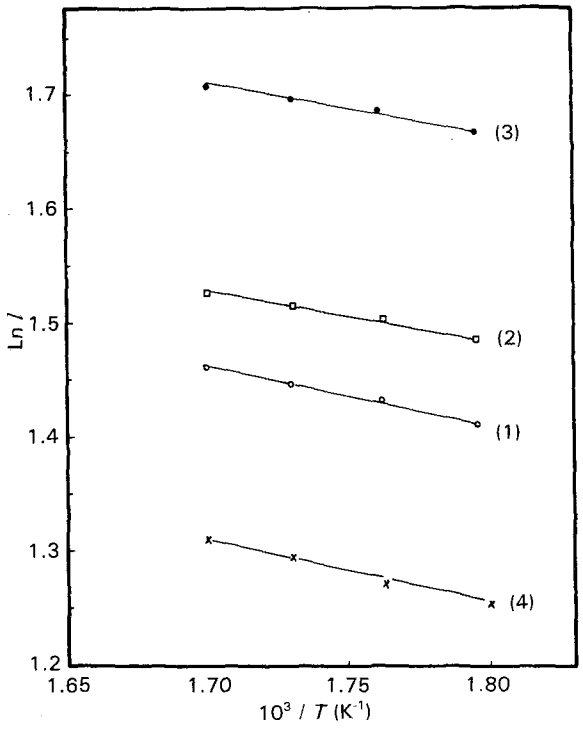

Figure 5 Relationship of $\ln I$ versus $1000/T$ for ΔE (kJ mol^{-1}) determination: (1) $Ga_3Fe_5O_{12}$, (2) $Ga_2AlFe_5O_{12}$, (3) $GaAl_2Fe_5O_{12}$ and (4) $Al_3Fe_5O_{12}$ garnets.

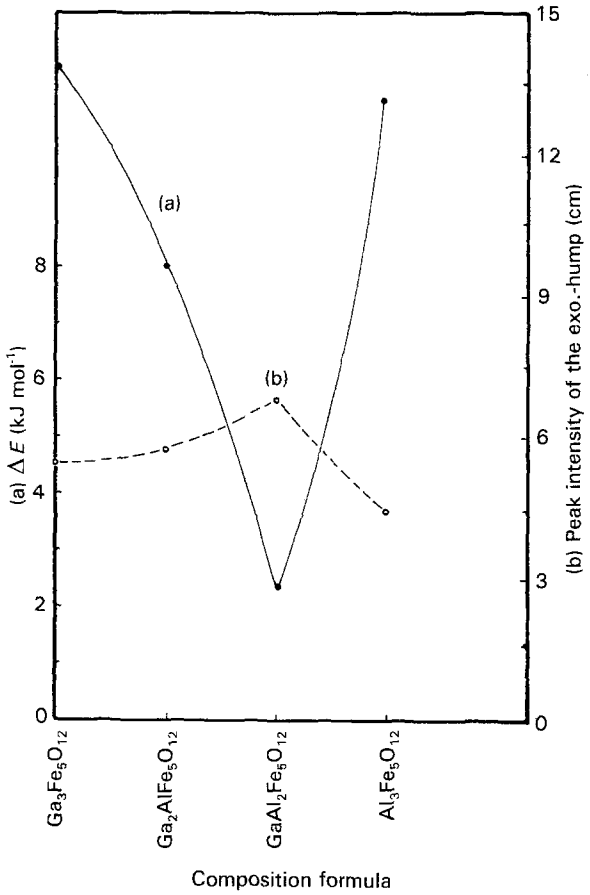

Figure 6 The variations of activation energy for (a) thermal change and (b) intensity (cm) of the broad DTA hump corresponding to heat capacity, as a function of garnet composition.

The behaviour of differential thermal analysis (DTA) curves is shown in Fig. 4. The patterns show as a general, common, trend that all investigated garnets possess a great thermal stability up to 1000 °C. However, weak endothermic peaks can be traced for all samples in the temperature range 70–80 °C which could be attributed to the dehydration of humidity water content. Such endothermic peaks seem to decrease as the aluminium content increases, indicating the less hygroscopic nature of aluminium-doped garnets and aluminium-garnet. All samples show a very broad hump extending all over the investigated range of temperature. This could be ascribed to lattice rearrangement and/or change in the observed high heat capacity of the investigated garnets, i.e. substitutional and not a structural phase change. The order of the thermal reaction was determined from the observed changes in DTA curves as the heating rate is changed, i.e. from the symmetry of the DTA curve. The symmetry of the peak is a/b and the reaction order, n, is determined using the Reich [9] empirical relation of the form

$$\text{reaction order, } n = 1.26\left(\frac{a}{b}\right)^{1/2} \quad (3)$$

where a/b is the peak shape factor.

The activation energy for such thermal changes, ΔE, for all samples is determined using the Piloyan *et al.* [10] method regarding the precautions of Lasoka [11]. As shown from Fig. 6 and Table III the activation energy (ΔE, kJ mol^{-1}) was found to decrease throughout substitution of Ga^{3+} with Al^{3+} cations down to a minimum value corresponding to the composition $GaAl_2Fe_5O_{12}$ which agrees well with the substitution mechanism, after which it rises. Further support for this deduction is evident from Fig. 6b indicating that Al^{3+} substitution in place of Ga^{3+} considerably increases the heat capacity of garnets up to a maximum value corresponding to the $GaAl_2Fe_5O_{12}$ composition, then it falls again. This is in conformity with results deduced from the present X-ray part. Regarding the reaction order data (see Table III), it is clear that the insertion of Al^{3+} cations into the garnet lattice does not alter the mechanism of solid state lattice rearrangement. However, the composition $GaAl_2Fe_5O_{12}$ has the highest reaction order (1.13). From the foregoing thermal analysis, it seems that the composition $GaAl_2Fe_5O_{12}$ differs from the others and may represent the most strained lattice. This conclusion is supported by its lowest activation energy for thermal change (1.59 kJ mol^{-1}) and its relatively large deviation from unity or from clean first-order reaction (1.13). Of course, lattice defects enhance the high-temperature solid-state reaction (phase change) which must be a diffusion-dependent process [12].

References

1. A. N. PETROV, G. V. DEMISOV and V. M. ZHUKOVKII, *Akad. Nauk SSSR Neorg. Mater.* **78** (1986) 663.
2. L. D. DISSADO and R. M. HELL, *J. Phys. Chem.* **14** (1981) L649.
3. K. SURESH and N. R. S. KUMAR, *Ilunheim Feol Repub. Ger.* **3** (1991) 148 (Patent).

4. S. GELLER, *Appl. Phys.* **31** (1960) 305.
5. F. A. MILLER and C. H. WIKINS, *Anal. Chem.* **24** (1952) 1253.
6. H. MOENKE, "Mineralspecktren II" (Acaodemine, Berlin, 1962).
7. K. A. WICKERSHEIM, R. A. LEFEVER and B. M. HANKING, *J. Chem. Phys.* **32** (1960) 271.
8. J. LAMBERT BATES and JOHN E. GARNIER, *J. Am. Ceram. Soc.* **64** (1981) C138.
9. L. REICH, *J. Inorg. Nucl. Chem.* **28** (1966) 1329.
10. G. O. PILOYAN, J. RYABCHIKOV and O. S. NOVIKOVA, *Nature* **212** (1966) 1229.
11. M. LOSOKA, *J. Therm. Anal.* **16** (1979) 197.
12. E. ELSHEREAFY and M. A. ABD EL-GHAFFAR, *Thermochim. Acta.* **186** (1991) 179.

Received 24 May
and accepted 10 December 1993